Dual-Mode Polarization Control with Quasi-Bound States in the Continuum

Luca Fagiani, Luca Bolzonello, Johann Osmond, Domenico de Ceglia, Niek van Hulst, Monica Bollani, and Maria Antonietta Vincenti*

Full control of light polarization is one of the most sought-after functionalities in nanophotonics since it allows the replacement of bulky optical components like wave retarders. Here, the study reports the theoretical and experimental demonstration of an ultra-compact dual-mode frequency selective polarization controller that leverages the topological features of symmetry protected quasi-bound states in the continuum (q-BICs) supported by a silicon-based nanostructure. Thanks to q-BIC resonances, arbitrarily polarized incoming light can be converted into linearly polarized light without resorting to the local phase tuning mechanisms that characterize optical metasurfaces. Moreover, the dual-mode operating regime allows to select the transmitted polarization without modifying the device orientation, therefore overtaking the concept of the wire grid polarizer. The experimental findings show that the proposed meta-polarizer possesses an extinction ratio of ≈40 dB for two linear cross-polarization excitations. These results pave the way for a novel class of ultra-compact devices that can be used to compensate unwanted birefringence in optical fibers or to control polarization in complex media environments.

L. Fagiani
Department of Physics
Politecnico di Milano
Piazza Leonardo da Vinci, 32, Milan 20133, Italy

L. Fagiani, M. Bollani
Istituto di Fotonica e Nanotecnologie-Consiglio Nazionale delle Ricerche (IFN-CNR), LNESS
Via Francesco Anzani, 42, Como 22100, Italy

L. Bolzonello, J. Osmond, N. van Hulst
ICFO-Institut de Ciencies Fotoniques
The Barcelona Institute of Science and Technology
av. Carl Friedrich Gauss, 3, Castelldefels, Barcelona 08860, Spain

D. de Ceglia, M. A. Vincenti
Department of Information Engineering
University of Brescia
Via Branze 38, Brescia 25123, Italy
E-mail: maria.vincenti@unibs.it

N. van Hulst
ICREA, Institució Catalana de Recerca i Estudis Avançats
Passeig de Lluís Companys, 23, Barcelona 08010, Spain

1. Introduction

Effective manipulation of light polarization is of utmost importance for a variety of applications including quantum communications, sensing, imaging, and material characterization, to name a few.[1] A straightforward approach to convert any incoming polarization into an arbitrary one consists in cascading quarter waveplates where the optical axes can be tilted at will. Although very effective in a laboratory environment, this methodology fails when trying to work with chip-scale optical components. In fact, achieving full control over polarization at the nanoscale is still a non-trivial task. Numerous solutions have been proposed over the years, all aimed at reducing device dimensions.[2] For this reason, efforts devoted to polarization detection and engineering have flourished in the last few years since the concept of metasurfaces has been introduced.[3] A carefully designed 2D arrangement of nanoparticles can in fact provide the necessary phase change to rotate linear polarization,[4] generate, modify, or preserve the handedness of circularly polarized light[5] as well as decode polarization properties or provide polarimetric imaging.[3c,6] However, one of the main limitations of current metasurface-based polarizers is that they rely on local phase tuning of their individual elements so that their design must be tailored based on the characteristics of the incoming light, namely frequency and polarization state. Here we present an ultracompact all-dielectric meta-polarizer that converts any incoming polarization into linear polarization without any predetermination of the incoming state of light. Polarization conversion is performed thanks to the excitation of symmetry-protected quasi-bound states in the continuum (q-BICs)[7] that can be excited in a properly designed silicon on insulator (SOI) nanostructure. Differently from their traditional metasurface counterparts which mimic the behavior of quarter waveplates, q-BICs do not exploit an engineered phase delay profile and can therefore robustly block specific polarization components regardless of the incoming polarization. The meta-polarizer also differs from traditional wire-grid linear polarizers since it could in turn suppress two orthogonal polarizations without changing the orientation of its elements. We then theoretically predict and experimentally demonstrate how the same device achieves an extinction ratio of ≈40 dB for two linearly cross-polarized beams. These results pave
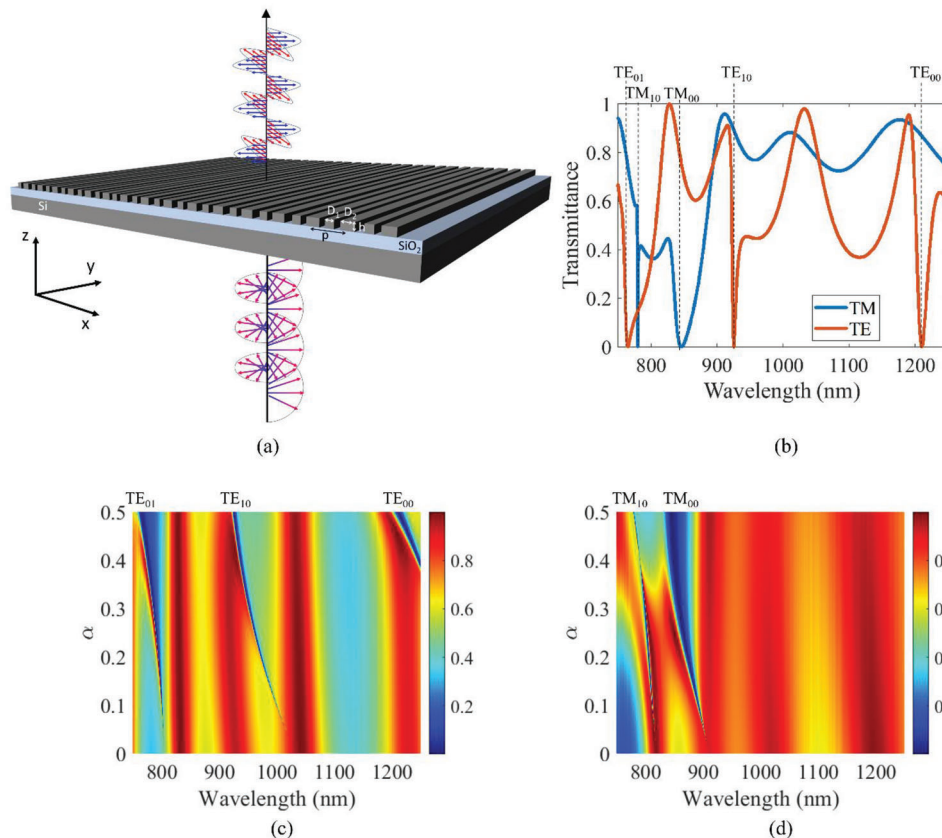
Figure 1. a) Working principle of the frequency selective polarization controller: a silicon-based nanostructure supporting q-BICs converts arbitrarily polarized incoming light into linearly polarized light; b) Transmission spectra for incoming TE (red line – electric field oriented along y) and TM (blue line – electric field oriented along x) polarizations for the following parameters: periodicity $p = 500$ nm, nanowire widths D1 = 175 nm and D2 = 87.5 nm (corresponding to an asymmetry factor $\alpha = 0.5$ and a FF = 0.7), and height $h = 145$ nm. SiO2 layer is 2 μm and Si substrate is 500 μm. For this parameters combination five q-BICs can be identified in the frequency range under investigation. Transmittance at normal incidence as a function of wavelength and asymmetry factor α for c) TE (electric field polarized along x) and d) TM (electric field polarized along y) polarized incoming light. Q-BIC modes appear in the radiation continuum, and they all undergo a blueshift as the asymmetry factor increases. All q-BICs become sharper and eventually disappear as the asymmetry factor vanishes, indicating the transition from q-BIC to BIC condition.

the way for a class of ultra-compact dual-mode optical devices that can be easily integrated into up-to-date on-chip technologies to provide efficient polarization control over a widely tunable frequency range.

2. Meta-Polarizer Working Principle

Photonic bound states in the continuum (BICs) are non-radiating states hidden in the continuum of propagating modes.[7–8] These dark modes possess a singular quality factor and virtually infinite lifetime that in turn guarantees extremely high field localization values at the nanoscale. For this reason, photonic BICs have been extensively investigated in different optical systems and for numerous applications that span from photo-detection and sensing to quantum and nonlinear optics.[9] Due to their bound nature, BICs cannot be excited in practical settings but they can be accessed once they have been coupled to the radiation channel as q-BICs.[10] Different type of q-BICs can be excited in optical systems, either triggered by the alteration of the structural parameters of the system, namely symmetry protected (SP) BICs,[7,11]

or by the accidental crossing of two resonant modes of the system, known as Friedrich-Wintegen (FW) or accidental BICs.[12] In all their forms, BICs and their leaky counterparts, q-BICs, are characterized by peculiar topological features that allow the manipulation of light at the nanoscale level. The same topological features allow to overcome the main limitation of metasurfaces to control light polarization: since q-BICs do not rely on the phase delay introduced by each element in the nanostructure, they can effectively block any incoming polarization that is not allowed by the specific q-BIC state. Moreover, q-BIC modes exhibit extremely sharp spectral features that can be easily tuned by changing the asymmetry factor of the nanostructure.

A silicon-based nanostructure where symmetry is properly altered by changing the width of every other element in the array (**Figure 1**a) can support several q-BIC modes. Those modes originate from their BICs counterparts that can be easily identified by performing an eigenmode analysis of the nanostructure before any asymmetry is introduced (see Note S1, Supporting Information), showing that the spectral location of those modes is expected to blue-shift as the asymmetry is introduced in the
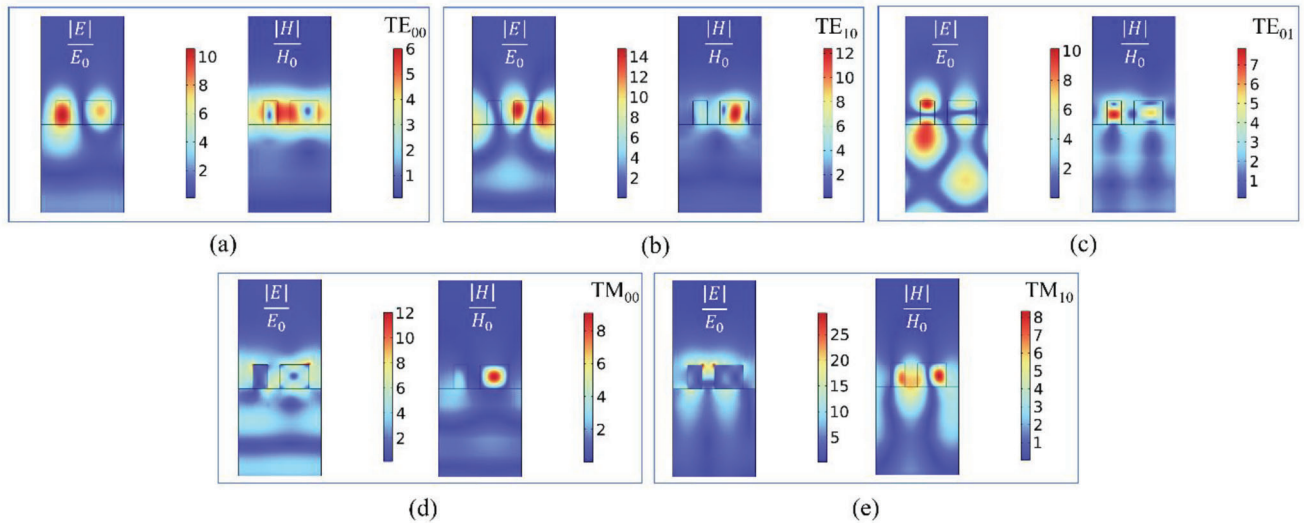
**ADVANCED
SCIENCE NEWS**

www.advancedsciencenews.com

**ADVANCED
OPTICAL
MATERIALS**

www.advopticalmat.de

Figure 2. Electric and magnetic field enhancement with respect to the incoming fields for a) TE_{00} q-BIC ($\lambda = 1211$ nm), b) TE_{10} q-BIC ($\lambda = 926$ nm), c) TE_{01} q-BIC ($\lambda = 764$ nm), d) TM_{00} q-BIC ($\lambda = 846$ nm) and e) TM_{10} q-BIC ($\lambda = 780$ nm). All field distributions present the high field localization inside the nanostructure that is expected from q-BIC modes. Field localization in panel (e) also reveals the interaction of the q-BIC with a leaky guided mode resonance associated with the onset of the first diffraction order of the periodic structure.

system and the modes transition from BICs to their radiative counterparts q-BICs. By simply scaling the size of the nanostructure's unit cell, q-BIC modes can be tuned almost at will across the electromagnetic spectrum.[13] As an example, here we investigate a device with five q-BIC modes in the near-IR frequency range (Figure 1b). The meta-polarizer is therefore composed of a set of silicon nano-bars with periodicity p = 500 nm, widths $D_1 = 175$ nm and $D_2 = D_1(1-\alpha) = 87.5$ nm [where we assume the asymmetry factor $\alpha = 0.5$ and the term $(1-\alpha)$ indicates the ratio of the nanobars' widths D_2/D_1] and height h = 145 nm, placed on top of 2 µm-thick SiO_2 layer and a Si substrate, where the real and imaginary part of silicon dielectric permittivity are taken from Reference.[14] Each of the q-BIC modes that can be supported in this nanostructure possesses a unique topological field distribution that eventually translates into a different device functionality. More specifically we can identify three q-BICs when the structure is excited with transverse electric (TE) polarization (electric field polarized along the y-axis) and two q-BICs for transverse magnetic (TM) polarization (electric field polarized along the x-axis). Although all these modes disappear when the geometrical symmetry is restored (Figure 1c,d) and can therefore be classified as SP q-BICs, only the modes labeled TE_{00}, TE_{01}, TM_{00} and TM_{10} in Figure 1b completely disappear in the perfectly symmetric structure, while mode TE_{10} can still be detected in the symmetric geometry by observing the transmission spectrum of the nanostructure off the Γ point (Note S2 and Figure S2, Supporting Information). Here q-BIC modes were classified based on the number of nodes inside the silicon nano-bars in the z or x direction.[15]

All resonant modes exhibit the distinctly high field enhancement that characterizes q-BICs (**Figure 2**) and a quality factor Q that depends on their interference with the Fabry-Pérot resonances supported by the SiO_2 layer (see Note S2, Supporting Information). We also note how for some of these resonances the electric and magnetic field distributions clearly resemble the topology of electric and magnetic dipoles or quadrupoles (see

Figure 2a,c,d), while other q-BIC modes present either a field distribution that is tilted with respect to the geometry (Figure 2b) or a field distribution that is the result of the hybridization of the q-BIC mode with a leaky guided mode resonance associated with the onset of the first diffraction order of the periodic structure (Figure 2e).

Regardless of which q-BIC mode is excited, the nanostructure can convert an arbitrarily polarized field into a linearly polarized one (either TE or TM) without any pre-determination of the incoming polarization nor by modifying the orientation of its elements as required in traditional wire-grid polarizers. The ability of the nanostructure to effectively manipulate the incoming light has been characterized by monitoring the transmitted polarization at each q-BIC resonance for different incoming polarization. Both impinging and transmitted polarizations were converted into Stokes parameters and plotted on the Poincaré sphere for easier reading (**Figure 3**). Four representative incoming polarization were considered: a) left-handed circularly polarized light with Stokes vector [1 0 0 1] (dark blue dot in Figure 3a); b) right-handed circularly polarized light with Stokes vector [1 0 0 -1] (dark blue dot in Figure 3b); c) an elliptical polarization with Stokes vector [1 0.88 0 −0.47] (dark blue dot in Figure 3c); and d) an elliptical polarization with Stokes vector [1 0.13 0.7 0.7] (dark blue dot in Figure 3d). For all q-BICs we can see how the incoming polarization is converted in either horizontal (point marked H in Figure 3, corresponding to an electric field polarized along x – TM polarization) or vertical (point marked V in Figure 3, corresponding to an electric field polarized along y – TE polarization). A slight deviation from perfectly vertical transmitted polarization is found for the TM_{10} resonance, which indeed suffers from a low transmission contrast with its orthogonal polarization (see Figure 1b), and it does not perfectly convert the incoming polarization into a linear one.

We stress that q-BICs perform the polarization conversion without resorting to individually designed phase-delay elements
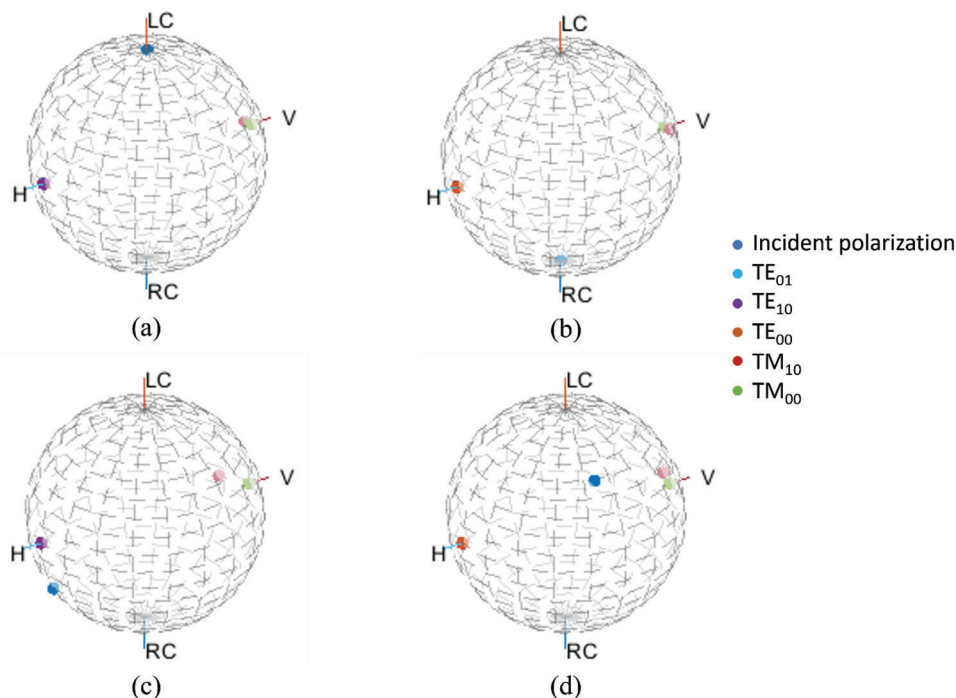
Figure 3. Schematic representation on the Poincaré sphere of the principle of operation of the silicon-based meta-polarizer. Four different incoming polarization have been tested to check if q-BIC modes were able to convert the incoming light into a linearly polarized field. On each sphere the incoming polarization is represented by the dark blue dot, while the transmitted polarization is represented with a different color depending on the excited mode. We stress that the dots associated with all TE resonances, namely purple, orange, and light blue dots, are not all visible since they are perfectly overlapped on the sphere. In other words, when the incoming light is perfectly tuned at those three resonances (TE_{00}, TE_{10} and TE_{01}) the nanostructure produces an outcoming light which is horizontally polarized. Tested incoming polarizations are: a) right-handed circular polarization, b) left-handed circular polarization, c) elliptical polarization with Stokes vector [1 0.88 0 −0.47] and d) elliptical polarization with Stokes vector [1 0.13 0.7 0.7].

as in traditional metasurfaces and they can provide extremely selective frequency polarization control by completely rejecting all unwanted polarization components. This ensures that the polarization control is robust and can be eventually tuned across the electromagnetic spectrum by playing with the asymmetry factor of the whole nanostructure. On the other hand, we note that the meta-polarizer works as described only at the wavelengths of the q-BIC modes, while for all other off-resonance wavelengths we can expect to detect a generic elliptical polarization as the output of our system regardless of the input polarization profile. The operating bandwidth of the system is, therefore, limited by the bandwidth of each mode. More specifically, our theoretical analysis (see Figure 1b) indicates the five q-BIC modes have the following full width at half maximum (FWHM) values: $FWHM_{TE01} \approx 34$ nm, $FWHM_{TE10} \approx 7$ nm, $FWHM_{TE00} \approx 15$ nm, $FWHM_{TM10} \approx 1$ nm, $FWHM_{TM00} \approx 38$ nm.

3. Fabrication of Dual-Mode Polarization Platform

The silicon-based nanostructure has been fabricated following the design criteria mentioned above. The nanopatterning steps include standard electron-beam lithography (EBL) and subsequent inductively coupled plasma – reactive ion etching (ICP-RIE) step.[16] The structures are fabricated on an SOI (001) wafer with a thickness of 145 nm on a SiO_2 box of 2 µm over a thick Si bulk (**Figure 4**a,c,d). A single layer of positive resist (PMMA) is

spin-coated on SOI to achieve a thickness of 80 nm and then it is patterned via EBL to generate the desired pattern with acceleration voltage of 30 kV. The used dose is 330 µC cm^{-2}. After the development in a 1:3 MIBK/IPA solution for 90 s, 45 nm of silica are deposited via e-beam evaporation to create, after the lift-off process, a hard mask. The regular patterns on the SOI are obtained thanks to an ICP-RIE machine using C_4F_8 and SF_6 as etchant gases. The SiO_2 mask is removed with a quick passage (20 sec) in a 5% in vol HF solution. The back part of the sample is then lapped with mechanical polishing to improve transmission measurement. The remaining organic contaminants are then eliminated with a 10 min bath in hot acetone and isopropanol followed by a cleaning in an oxygen plasma.

4. Results and Discussion

Transmission spectra from the meta-polarizer have been simulated (**Figure 5**a) and experimentally measured (Figure 5b) for normal incidence conditions and rotating linear polarization (electric field rotates in the x,y plane from 0° – TE polarization – to 90° – TM polarization). A homemade transmission optical setup is used for the characterization (Figure 4b). The laser source is a broadband Ti:Sapphire oscillator laser with 85 MHz repetition rate (Thorlabs Octavius) with broadband spectrum (640–940 nm). A linear polarizer is used to clean the polarization of the incoming radiation, followed by a tunable band-pass filter with
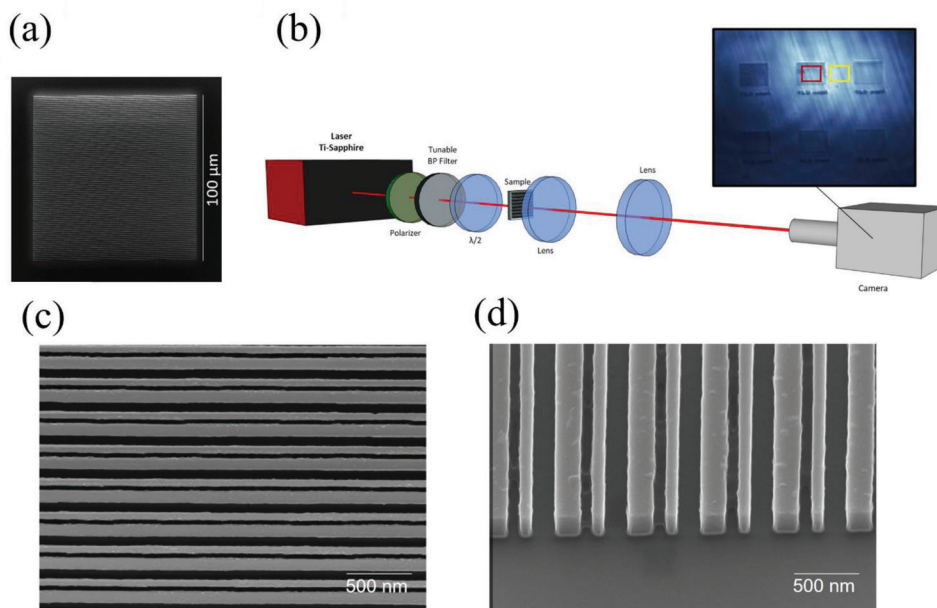
**ADVANCED
SCIENCE NEWS**

www.advancedsciencenews.com

**ADVANCED
OPTICAL
MATERIALS**

www.advopticalmat.de

Figure 4. SEM characterization in top-view of the overall a) 100 µm² Si device. b) Sketch of the optical setup, with a highlight on the main optical features used. Inset shows an example of an image taken with the CCD; Zoom of the inner region of the nanostructure from c) top and d) tilted view.
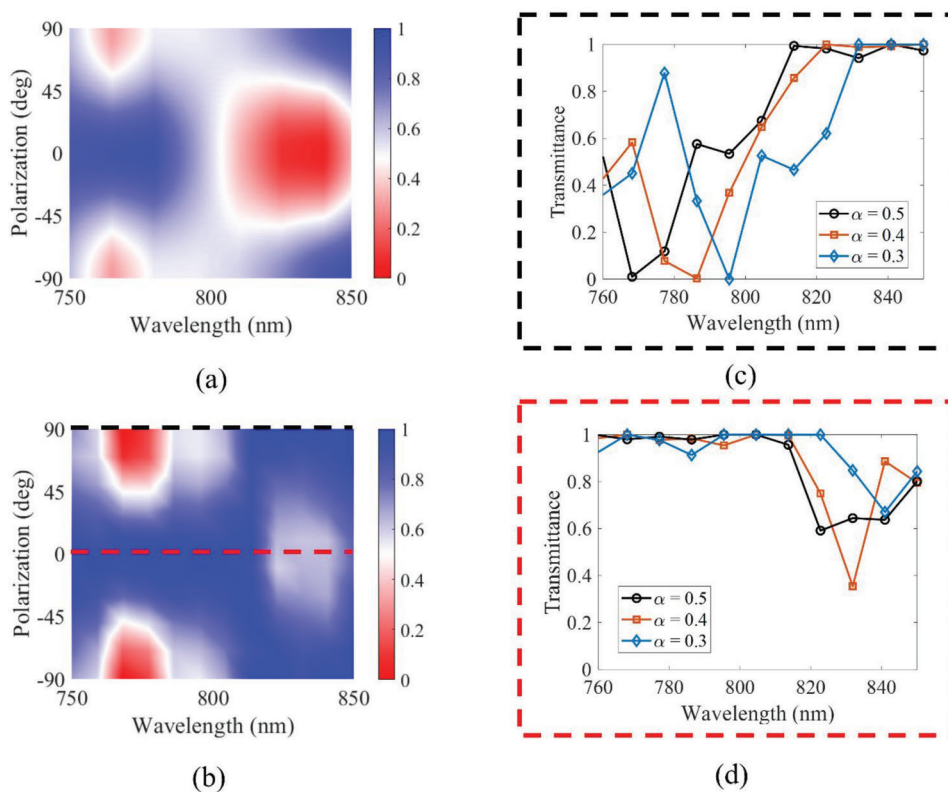

Figure 5. a) Simulated and b) measured transmission spectra for an incoming linear polarization impinging at normal incidence. Polarization rotation indicates a transition from a linearly polarized electric field along x (TM polarization – 0°) to a linearly polarized electric field along y (TE polarization – 90°). Measured transmission spectra for different asymmetry factors for a linear incoming polarization along c) x – 0° and d) y – 90°. The spectral resolution and bandwidth limitation of the detection system allowed the observation only of the modes labeled TM_{00} and TE_{01} of Figure 1b. Note: the experimental data in panels (b), (c), and (d) have been normalized to 1 to make an easier comparison with the theoretical simulations that assume a much shorter Si substrate for the sample.

**ADVANCED
SCIENCE NEWS**

www.advancedsciencenews.com

**ADVANCED
OPTICAL
MATERIALS**

www.advopticalmat.de

12 nm of bandwidth. A half wave-plate tunes the polarization orientation. The sample is illuminated on the backside with a 0.01 NA obtained with an achromatic lens of focal 20 mm. The sample is imaged with a 4-f system into an Andor iXon EMCCD camera. In this way, the sample can be identified, and the transmitted signal collected at the same time. A slight discrepancy between the theoretical and experimental spectral position of the resonances can be attributed to deviations in the fabrication profiles with respect to the simulated structures.[16b]

Such discrepancy is more pronounced for the TM_{00} mode than for the TE_{10} mode, as also confirmed by our numerical analysis on fabrication errors' tolerance (see Note S3, Supporting Information). To confirm the sensitivity of these resonances on the geometrical parameters we fabricated and tested more nanostructures with identical periodicity and slightly different structural asymmetry (nominal asymmetry factors from $\alpha = 0.3$ to $\alpha = 0.5$): a strong blue shift of all q-BICs is observed as the asymmetry factor increases, suggesting that the meta-polarizer operating regime can be easily tuned by properly choosing the asymmetry factor between the nano-bars (Figure 5c,d).

Finally, we compared the theoretical predictions and measurements of the meta-polarizer extinction ratio for two orthogonal linearly polarized beams. The extinction ratio is calculated as the ratio of the transmittance at 0° (electric field along x – TM polarization) and 90° (electric field along y – TE polarization) of polarization rotation in the x,y plane.

Each transmittance in the experimental data is then in turn calculated as the ratio of the laser intensity through the nanostructures and outside. More specifically, we average pixels values inside and outside the structure (respectively red square and yellow square in the inset of Figure 4b), in regions with constant laser intensities:

$$ER = \frac{T_{0°}}{T_{90°}} = \frac{T_{TM}}{T_{TE}} \tag{1}$$

$$T = \frac{I_{out}}{I_{in}} = \frac{\bar{I}_{px_{out}}}{\bar{I}_{px_{in}}} \tag{2}$$

Figure 6 shows how experimental results can be well superimposed with our numerical prediction and how the meta-polarizer experimentally yields a constant extinction ratio of ≈40 dB for different asymmetry factors. We also note that, while the spectral shift for different asymmetry parameters is consistent between theory and experiment, the low experimental spectral resolution does not allow to properly detect the maximum achievable extinction ratio and the minimum in the extinction ratio associated with the TM_{10} mode. Moreover, the absence in the experimental spectra of the TM_{10} mode can be also ascribed to the higher sensitivity of this mode to fabrication defects, as confirmed by the numerical analysis in Note S3 (Supporting Information). In other words, while TE_{10} mode is more robust to fabrication defects, the TM_{10} mode undergoes a more pronounced spectral shift when fabrication parameters are changed by the same amount. This translates into less pronounced measured spectral features and, in turn, in a lower contrast between two orthogonal polarization transmission values. Thanks to the measurements of the extinction ratio for the different asymmetry factors we were able to infer the difference between the nominal asymmetry associated
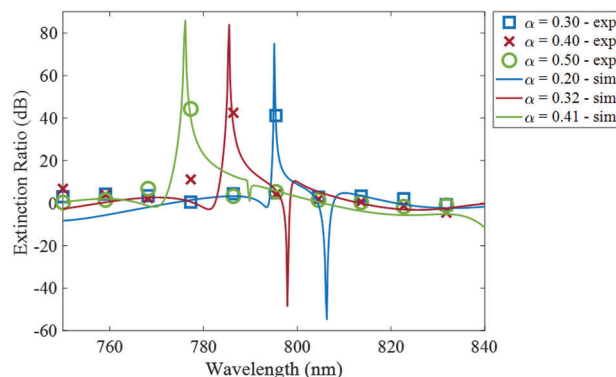

Figure 6. Simulated (solid lines) and measured (markers) extinction ratio for two orthogonal linearly polarized beams impinging at normal incidence on three silicon-based nanostructures with different asymmetry factors. We note that proper fit of the experimental data is possible only assuming a reduction from the nominal asymmetry factor for the fabricated nanostructures as indicated in the legend for the simulated curves.

with the fabricated samples and the actual asymmetry factor of the structure. More specifically the theoretical fit allows to estimate a reduction in the effective asymmetry parameter of ≈0.1. Such reduction is consistent for all tested nanostructures and provides good feedback on the fabrication process. A comparison of the theoretical and experimental polarizer conversion efficiency (Note S4, Supporting Information) also confirms that the TE_{01} mode guarantees a much higher conversion efficiency than the TM_{00} mode.

5. Conclusion

In summary, we demonstrated how the excitation of SP q-BICs in a silicon-based nanostructure can be exploited to convert a randomly polarized incoming beam into either a TM or a TE linearly polarized field depending on the chosen operating frequency. Such dual-mode operation, which cannot be realized with metasurfaces that rely on specifically designed phase-delay elements or with traditional wire-grid polarizers, provides an exceptional tool to replace both bulky and ultrathin wave retarders. Our results also suggest that this novel class of meta-polarizers will allow for a full polarization control over a widely tunable frequency range thanks to the scalability of their elements and the fine tunability induced by the asymmetry factor of the nanostructure.

Supporting Information

Supporting Information is available from the Wiley Online Library or from the author.

Acknowledgements

Conflict of Interest

The authors declare no conflict of interest.

Data Availability Statement

The data that support the findings of this study are available from the corresponding author upon reasonable request.

[1] a) J. C. Bose, *Proc. Royal Soc* **1898**, *63*, 146; b) G. B. Xavier, G. Vilela De Faria, G. P. Temporão, J. P. Von Der Weid, *Opt. Express* **2008**, *16*, 1867; c) D. Cozzolino, B. Da Lio, D. Bacco, L. K. Oxenløwe, *Adv. Quantum Technol.* **2019**, *2*, 1900038; d) D. Neshev, I. Aharonovich, *Light: Sci. Appl.* **2018**, *7*, 58; e) M. Sukharev, T. Seideman, *Nano Lett.* **2006**, *6*, 715; f) J. S. Tyo, D. L. Goldstein, D. B. Chenault, J. A. Shaw, *Appl. Opt.* **2006**, *45*, 5453; g) E. Laux, C. Genet, T. Skauli, T. W. Ebbesen, *Nat. Photonics* **2008**, *2*, 161; h) A. Pierangelo, A. Benali, M.-R. Antonelli, T. Novikova, P. Validire, B. Gayet, A. De Martino, *Opt. Express* **2011**, *19*, 1582; i) M. Losurdo, M. Bergmair, G. Bruno, D. Cattelan, C. Cobet, A. De Martino, K. Fleischer, Z. Dohcevic-Mitrovic, N. Esser, M. Galliet, R. Gajic, D. Hemzal, K. Hingerl, J. Humlicek, R. Ossikovski, Z. V. Popovic, O. Saxl, *J. Nanoparticle Res.* **2009**, *11*, 1521.

[2] a) Y. Guo, M. Xiao, S. Zhou, S. Fan, *Adv. Opt. Mater.* **2019**, *7*, 1801453; b) I. Sinev, I. Iorsh, A. Bogdanov, D. Permyakov, F. Komissarenko, I. Mukhin, A. Samusev, V. Valuckas, A. I. Kuznetsov, B. S. Luk'yanchuk, A. E. Miroshnichenko, Y. S. Kivshar, *Laser Photonics Rev.* **2016**, *10*, 799; c) P. Ginzburg, F. J. R. Fortuño, G. A. Wurtz, W. Dickson, A. Murphy, F. Morgan, R. J. Pollard, I. Iorsh, A. Atrashchenko, P. A. Belov, Y. S. Kivshar, A. Nevet, G. Ankonina, M. Orenstein, A. V. Zayats, *Opt. Express* **2013**, *21*, 14907; d) T. Liu, A. R. Zakharian, M. Fallahi, J. V. Moloney, M. Mansuripur, *IEEE Photonics Technol. Lett.* **2005**, *17*, 1435; e) S. J. Elston, G. P. Bryan-Brown, J. R. Sambles, *Phys. Rev. B* **1991**, *44*, 6393; f) C. Huang, Y. Feng, J. Zhao, Z. Wang, T. Jiang, *Phys. Rev. B* **2012**, *85*, 195131; g) F. Ding, *Prog. Electromagn. Res.* **2022**, *174*, 55.

[3] a) N. Yu, F. Capasso, *Nat. Mater.* **2014**, *13*, 139; b) N. Yu, P. Genevet, M. A. Kats, F. Aieta, J.-P. Tetienne, F. Capasso, Z. Gaburro, *Science* **2011**, *334*, 333; c) A. Tognazzi, K. I. Okhlopkov, A. Zilli, D. Rocco, L. Fagiani, E. Mafakheri, M. Bollani, M. Finazzi, M. Celebrano, M. R. Shcherbakov, A. A. Fedyanin, C. De Angelis, *Opt. Express* **2021**, *29*, 11605; d) M. Kang, Z. Zhang, T. Wu, X. Zhang, Q. Xu, A. Krasnok, J. Han, A. Alù, *Nat. Commun.* **2022**, *13*, 4536; e) Y. Hu, X. Wang, X. Luo, X. Ou, L. Li, Y. Chen, Y. Ping, S. Wang, H. Duan, **2020**, *9*, 3755; f) K. Zhang, Y. Yuan, X. Ding, H. Li, B. Ratni, Q. Wu, J. Liu, S. N. Burokur, J. Tan, *Laser Photonics Rev.* **2021**, *15*, 2000351.

[4] a) Y. Ye, S. He, *Appl. Phys. Lett.* **2010**, *96*, 203501; b) L. Cong, W. Cao, X. Zhang, Z. Tian, J. Gu, R. Singh, J. Han, W. Zhang, *Appl. Phys. Lett.* **2013**, *103*, 171107.

[5] a) X. Chen, L. Huang, H. Mühlenbernd, G. Li, B. Bai, Q. Tan, G. Jin, C.-W. Qiu, S. Zhang, T. Zentgraf, *Nat. Commun.* **2012**, *3*, 1198; b) H. L. Zhu, S. W. Cheung, K. L. Chung, T. I. Yuk, *IEEE Trans. Antennas Propag.* **2013**, *61*, 4615; c) J. P. Balthasar Mueller, N. A. Rubin, R. C. Devlin, B. Groever, F. Capasso, *Phys. Rev. Lett.* **2017**, *118*, 113901; d) X. Wu, Y. Meng, L. Wang, J. Tian, S. Dai, W. Wen, *Appl. Phys. Lett.* **2016**, *108*, 183502; e) Y. Yuan, Q. Wu, S. N. Burokur, K. Zhang, *IEEE Trans Microw Theory Tech* **2023**, *71*, 3259.

[6] a) Y. D. Shah, A. C. Dada, J. P. Grant, D. R. S. Cumming, C. Altuzarra, T. S. Nowack, A. Lyons, M. Clerici, D. Faccio, *ACS Photonics* **2022**, *9*, 3245; b) Y. Intaravanne, X. Chen, *Nanophotonics* **2020**, *9*, 1003; c) D. Wen, F. Yue, S. Kumar, Y. Ma, M. Chen, X. Ren, P. E. Kremer, B. D. Gerardot, M. R. Taghizadeh, G. S. Buller, X. Chen, *Opt. Express* **2015**, *23*, 10272; d) J. P. Balthasar Mueller, K. Leosson, F. Capasso, *Optica* **2016**, *3*, 42; e) W. Wan, J. Gao, X. Yang, *Adv. Opt. Mater.* **2017**, *5*, 1700541; f) A. Pors, M. G. Nielsen, S. I. Bozhevolnyi, *Optica* **2015**, *2*, 716.

[7] C. W. Hsu, B. Zhen, J. Lee, S.-L. Chua, S. G. Johnson, J. D. Joannopoulos, M. Soljacic, *Nature* **2013**, *499*, 188.

[8] C. W. Hsu, B. Zhen, A. D. Stone, J. D. Joannopoulos, M. Soljacic, *Nat. Rev. Mater.* **2016**, *1*, 16048.

[9] a) S. Romano, G. Zito, S. Torino, G. Calafiore, E. Penzo, G. Coppola, S. Cabrini, I. Rendina, V. Mocella, *Photonics Res.* **2018**, *6*, 726; b) Y. Chen, C. Zhao, Y. Zhang, C.-W. Qiu, *Nano Lett.* **2020**, *20*, 8696; c) Y. Wang, Z. Yu, Z. Zhang, B. Sun, Y. Tong, J.-B. Xu, X. Sun, H. K. Tsang, *ACS Photonics* **2020**, *7*, 2643; d) L. Carletti, K. Koshelev, C. De Angelis, Y. Kivshar, *Phys. Rev. Lett.* **2018**, *121*, 033903; e) N. Bernhardt, K. Koshelev, S. J. U. White, K. W. C. Meng, J. E. Fröch, S. Kim, T. T. Tran, D.-Y. Choi, Y. Kivshar, A. S. Solntsev, *Nano Lett.* **2020**, *20*, 5309; f) Z. Liu, Y. Xu, Y. Lin, J. Xiang, T. Feng, Q. Cao, J. Li, S. Lan, J. Liu, *Phys. Rev. Lett.* **2019**, *123*, 253901; g) Y. Wang, B.-Y. Xie, Y.-H. Lu, Y.-J. Chang, H.-F. Wang, J. Gao, Z.-Q. Jiao, Z. Feng, X.-Y. Xu, F. Mei, S. Jia, M.-H. Lu, X.-M. Jin, *Light: Sci. Appl.* **2021**, *10*, 173; h) K. I. Okhlopkov, A. Zilli, A. Tognazzi, D. Rocco, L. Fagiani, E. Mafakheri, M. Bollani, M. Finazzi, M. Celebrano, M. R. Shcherbakov, C. De Angelis, A. A. Fedyanin, *Nano Lett.* **2021**, *21*, 10438.

[10] a) J. W. Yoon, S. H. Song, R. Magnusson, *Sci. Rep.* **2015**, *5*, 18301; b) A. C. Overvig, S. Shrestha, N. Yu, *Nanophotonics* **2018**, *7*, 1157.

[11] J. M. Foley, S. M. Young, J. D. Phillips, *Phys. Rev. B* **2014**, *89*, 165111.

[12] a) H. Friedrich, D. Wintgen, *Phys. Rev. A* **1985**, *32*, 3231; b) C. W. Hsu, B. Zhen, S.-L. Chua, S. G. Johnson, J. D. Joannopoulos, M. Soljačić, *Light: Sci. Appl.* **2013**, *2*, e84.

[13] L. Kühner, L. Sortino, B. Tilmann, T. Weber, K. Watanabe, T. Taniguchi, S. A. Maier, A. Tittl, *Adv. Mater.* **2023**, *35*, 2209688.

[14] M. A. Green, M. J. Keevers, *Prog. Photovoltaics* **1995**, *3*, 189.

[15] Y. Wang, J. Song, L. Dong, M. Lu, *J. Opt. Soc. Am. B* **2016**, *33*, 2472.

[16] a) A. Zilli, L. Fagiani, A. Tognazzi, E. Mafakheri, K. Okhlopkov, D. Rocco, M. Shcherbakov, A. Fedyanin, C. De Angelis, M. Finazzi, M. Celebrano, M. Bollani, *Il Nuovo Cimento* **2021**, *21*, 44; b) L. Fagiani, M. Gandolfi, L. Carletti, C. De Angelis, J. Osmond, M. Bollani, *Micro Nano Eng.* **2023**, *19*, 100187.